

Superfluid density and carrier concentration across a superconducting dome: the case of $\text{SrTi}_{1-x}\text{Nb}_x\text{O}_3$

Clément Collignon^{1,2}, Benoît Fauqué^{1,3}, Antonella Cavanna⁴, Ulf Gennser⁴, Dominique Mailly⁴ and Kamran Behnia¹

(1) *Laboratoire Physique et Etude de Matériaux (UMR 8213-CNRS), ESPCI, UPMC, PSL, F-75005, Paris, France*

(2) *Département de physique and RQMP, Université de Sherbrooke, Sherbrooke, Québec J1K 2R1, Canada*

(3) *JEIP, USR 3573 CNRS, Collège de France, PSL Research University,*

11, place Marcelin Berthelot, 75231 Paris Cedex 05, France

(4) *Laboratoire de Photonique et de Nanostructures, (UPR20-CNRS), F-91460 Marcoussis, France*

(Dated: February 17, 2017)

The critical temperature of a superconductor may evolve non-monotonically with carrier concentration. The fate of the superfluid density in this context has remained an unsettled issue for decades. Here, we present a study of the lower critical field, H_{c1} , of $\text{SrTi}_{1-x}\text{Nb}_x\text{O}_3$ as a function of carrier concentration with the aim of quantifying the superfluid density. At low carrier concentration (i.e. the underdoped side), superfluid density and the carrier concentration in the normal state remain equal within experimental margin. A significant deviation between the two numbers starts at optimal doping and gradually increases with doping. Reminiscent of cuprate superconductors, the inverse of the penetration depth and the critical temperature follow parallel evolutions. In the overdoped regime, the zero-temperature superfluid density becomes much lower than the normal-state carrier density before vanishing all together. We show that the density mismatch and the clean-to-dirty crossover are concomitant. Our results imply that the discrepancy between normal and superconducting densities is generic to the overdoped side of any superconducting dome.

A. Introduction

In many superconductors with an insulating parent, the critical temperature is a non-monotonic function of carrier concentration. Such superconducting domes are often found near an electronic order, which competes with superconductivity and may play a role in the formation of Cooper pairs. Their very existence raises a fundamental question. How does the superfluid density evolve in such a context? Does it remain equal to the concentration of electrons in the normal state? Or does it follow the non-monotonic variation of the critical temperature? Mostly debated in the context of high- T_c cuprates during the past few decades[1, 2], answers to these questions remain controversial, as shown by the conclusions of a recent study of the link between critical temperature and superfluid density in overdoped cuprates[3].

Among doped semiconductors with a superconducting ground state[4], SrTiO_3 [5–7] is distinguished by the precocity of its superconductivity. With only 10^{-5} electron per formula unit (f.u.)[6, 8], the system becomes superconducting. When carrier density exceeds 0.02/f.u., it ceases to be so[7, 9, 10]. This superconducting dome raises two distinct and still unanswered questions: how does superconductivity persist in the dilute limit in spite of a hierarchy inversion between Fermi and Debye temperatures? Why does it disappear on the overdoped side despite the steady increase in the electronic density of states?

On the other hand, the case of SrTiO_3 offers a unique opportunity to explore the behavior of superfluid density when the critical temperature is not a monotonic function of carrier density. Indeed, the superconducting instability occurs in a well-documented Fermi surface in which carrier concentration is known with a reliable accuracy[9]

and can be tuned across orders of magnitude. Here, we present an extensive study of the lower critical field in $\text{SrTi}_{1-x}\text{Nb}_x\text{O}_3$ across the superconducting dome with a focus on the relative magnitude of superfluid and normal-carrier density. In the underdoped regime, we find that the superfluid density extracted from the magnitude of the lower critical field is in excellent agreement with the carrier concentration in the normal state. Deep in the overdoped regime, a mismatch between the extracted superfluid density and the concentration of normal electrons is detectable and steadily increases with doping. We show that this mismatch is concomitant with the passage from clean to dirty limit. This conclusion has implications beyond the specific case of SrTiO_3 , and in particular for the more controversial case of cuprates[3, 11]. Comparing our data with what has been reported in Nb and optimally-doped YBCO, we find that in all three superconductors, when the system is clean, the penetration depth is indeed set by the ratio of carrier concentration to effective mass.

B. Results

We measured the lower critical field, H_{c1} , with Hall probes based on the 2D electron gas formed at an Al-GaAs/GaAs interface. Such a device can monitor local magnetization at micron scale and was used before to study vortex avalanches in superconducting niobium[12]. Similar Hall microprobes have been used before to measure H_{c1} in heavy-fermion[13] and in iron-based[14] superconductors. As shown in the inset of Fig.1.a, each probe is a $5 \times 5 \mu\text{m}^2$ square, $100 \mu\text{m}$ spaced from its immediate neighbor. The Hall resistance of the microprobe suddenly rises at the penetration field H_p (See Fig.1.a).

The intrinsic lower critical field, H_{c1} is proportional H_p . In the case of a platelet, the geometrical factor is:

$$H_{c1} = \frac{1}{\tanh(\sqrt{0.36t/w})} H_p \quad (1)$$

Where t and w are respectively the thickness and the width of the slab [15].

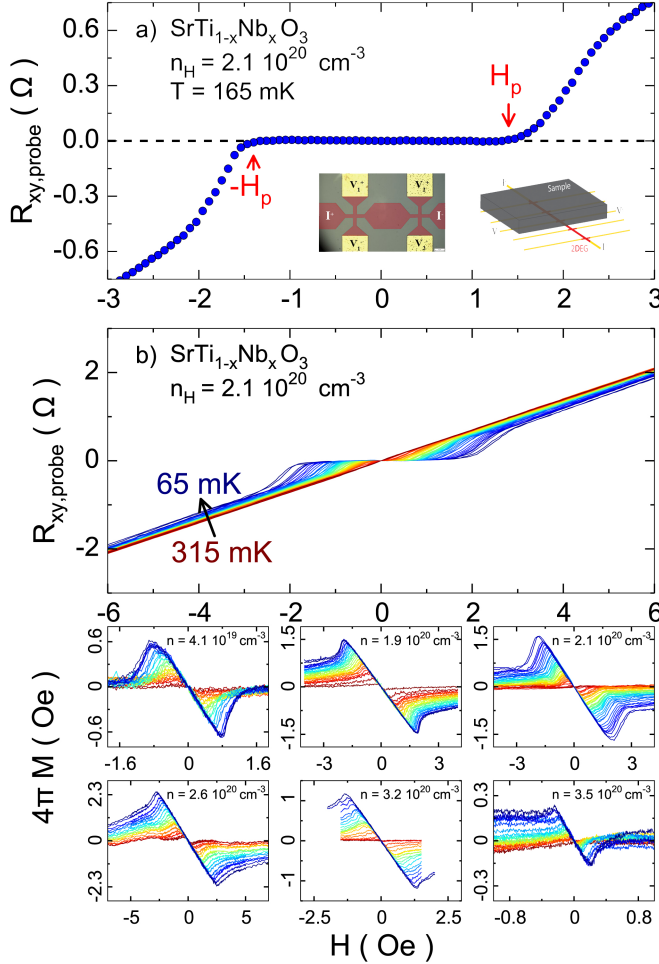


FIG. 1: **a**: Typical field dependence of the Hall resistivity of a microprobe with a superconducting sample above. The measured signal, directly proportional to the local magnetic field, suddenly rises when the first vortex penetrates the sample. The sharpness indicates the absence of surface-barrier effects or gradual vortex leak from sample corners[18]. The inset shows, in false colors, a picture of the array of Hall microprobes used for this experiment and a scheme of how a sample is mounted on the array of probes. **b**: Raw data for the $n_H = 2.1 \cdot 10^{20} \text{ cm}^{-3}$ sample at different temperatures. Bottom panels: Magnetization deduced from raw data for all six samples as a function of magnetic field.

For each sample, we performed measurements at different temperatures extending from $T_{base} \sim 30 - 50 \text{ mK}$ up to T_c and above, and extracted $H_p(T)$. The raw data

for $n_H = 2.1 \cdot 10^{20} \text{ cm}^{-3}$ is shown in Fig.1.b. The measured local field, B , can be used to extract magnetization through $M = B/\mu_0 - H$. In all six samples, magnetization is proportional to $-H$ at low field, sharply drops at H_p and decreases smoothly afterwards. Superconducting slabs with a small Ginzburg parameter typically behave in this way[16]. The magnitude of H_p and H_{c1} at each temperature can be determined unambiguously. The temperature dependence of H_{c1} for all six samples is exposed in Fig.2.a. Our results agree with what was reported in an early study on the lower critical field of two $\text{SrTi}_{1-x}\text{Nb}_x\text{O}_3$ samples near optimal doping[17]. As one can see in Fig.2.b, the doping dependence of H_{c1} and T_c are similar to each other. Both present a dome-like structure. This is our first result.

The lower critical field is intimately linked to magnetic penetration depth, λ . Roughly speaking, at H_{c1} the whole magnetic flux is contained by a single vortex of radius λ . A more elaborate treatment take in to consideration energy corrections due to the internal structure of the vortex including its normal core. For systems with Ginzburg parameter $\kappa \geq 5$, where κ is the ratio of the penetration depth λ over the superconducting coherence length ξ , H_{c1} is governed with negligible error by the following approximation [19–22]:

$$H_{c1} = \frac{\phi_0}{4\pi\lambda^2} (\ln(\kappa) + 0.5) \quad (2)$$

Here ϕ_0 is the quantum of magnetic flux. One can extract κ by measuring the two critical fields:

$$\frac{2\kappa^2}{\ln(\kappa) + 0.5} = \frac{H_{c2}}{H_{c1}} \quad (3)$$

We measured the bulk H_{c2} in four of our samples and found that $\kappa \simeq 7.5$ in the low doping level (when the system is in the clean limit) and increases steadily up to 15 with doping. This allowed us to extract the penetration depth from H_{c1} using Eq. 2. The superfluid density and the penetration depth are intimately linked to each other through the London equation[19]:

$$\lambda^{-2} = \mu_0 e^2 \frac{n_s}{m^*} \quad (4)$$

The doping dependency of λ^{-2} is shown in Fig.3. One can see that it closely follows the critical temperature, reminiscent of the case of cuprates[3, 11]. Uemura and co-workers[1] were the first to highlight the scaling between superfluid stiffness (defined as $\frac{n_s}{m^*}$) and the critical temperature in different superconductors.

In order to see what sets the magnitude of the penetration depth in a superconductor, let us now compare strontium titanate with two other superconductors (Fig.2b). The penetration depth is 870nm in optimally-doped strontium titanate and 31.5nm in niobium[31](in agreement with H_{c1} [32] and $\kappa \approx 0.85$ [33]). Given the large difference in their carrier concentration, this is not surprising. As seen in table 1, the extracted superfluid

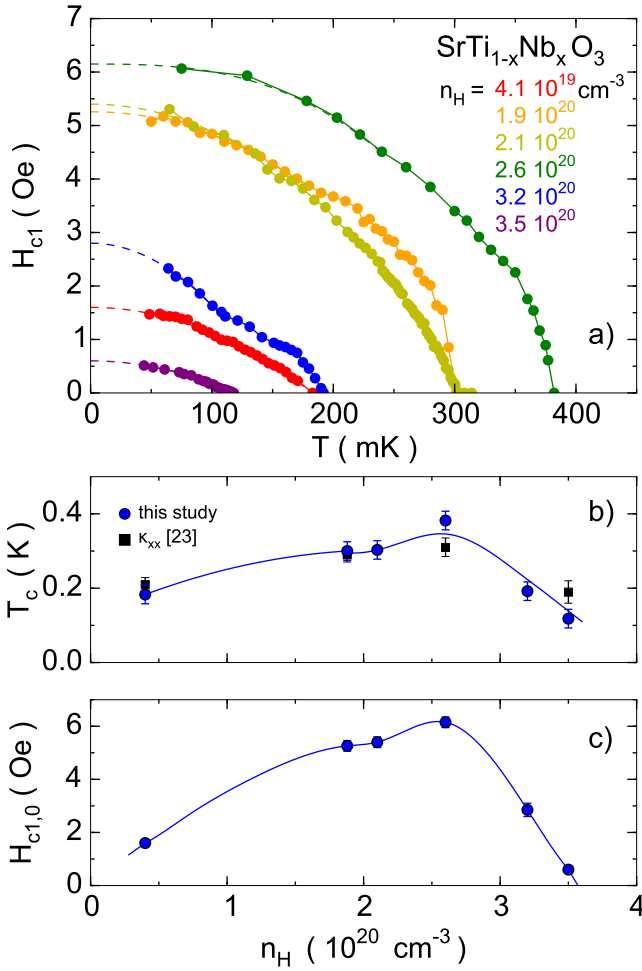


FIG. 2: **a:** Lower critical field vs temperature for all six samples deduced from H_p and geometrical correction of the demagnetization field. The dashed lines are extrapolations to $T \rightarrow 0$. **b:** Doping dependence of the critical temperature determined by Hall probe magnetometry (blue disks) and thermal conductivity (black squares)[23], the blue line is a guide to the eye. **c:** Doping dependence of H_{c1} , the blue line is a guide to the eye.

density is close to the carrier density according to the Hall coefficient. It is instructive to consider the case of YBCO near optimal doping. The measured λ (103 nm[37]) corresponds to what one expects given the Hall coefficient in the vicinity of optimal doping[41]. Clearly, what sets the magnitude of the penetration depth in a given superconductor is its carrier density (and not its critical temperature). This is the second message of this paper.

Multi-band superconductivity in strontium titanate can be a source of additional complication. An extensive study of quantum oscillation[9] found new frequencies emerging above two critical doping levels, a clear indication of distinct bands being successively filled upon doping, as expected by band calculations[24]. Thus, theory expects and experiment confirms that there are concentric Fermi-surface sheets all located at the center of

the Brillouin zone. Early tunneling studies[10] and more recent thermal conductivity measurements[23] detected two distinct gaps, indicating that at least two bands condensate. The cyclotron mass of the three bands are not the same. The lower band (or the outer sheet of the Fermi surface) is heavier ($m^* \approx 3.5 - 4m_e$) compared to the higher bands ($m^* \approx 1.3m_e$). These numbers are consistent with what was found by ARPES ($1.5m_e$ and $6m_e$) at a higher concentration[25]. Most carriers reside in the lower band, associated with the largest Fermi surface pocket, containing more than three-fourth of the total concentration[9]. Hence, one expects the average mass to be closer to the heavier one. This is confirmed by the specific heat data at optimal doping (that is $n_H = 2.6 \times 10^{20} \text{ cm}^{-3}$)[23]. The electronic specific heat, $\gamma = 1.55 \text{ mJ mol}^{-1} \text{ K}^{-2}$, is remarkably large for a dilute system and implies $m^* = 4.2m_e$ [23]. We have injected this value in to Eq.4, and deduced the superfluid density n_s for all samples, assuming a single-band picture.

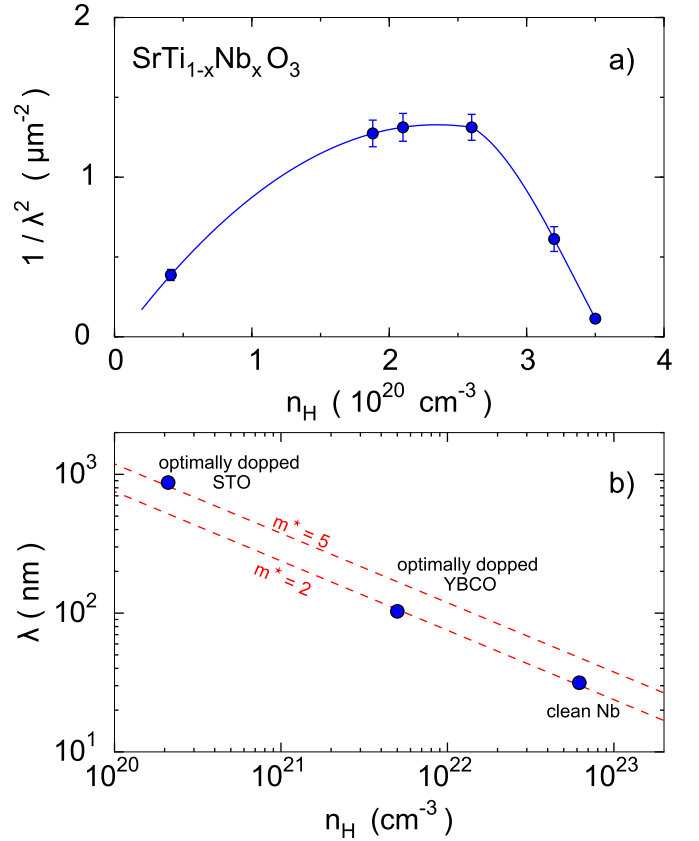


FIG. 3: **a:** Doping dependence of the penetration depth plotted as λ^{-2} vs n_H . It exhibits a dome-like structure comparable to T_c , as in the case of cuprates[11]. **b:** Penetration depth plotted as a function of n_H in three different superconductors. In the case of YBCO the symbol represents the Hall coefficient measured at $p=0.177$ [41] and the penetration depth along the a -axis measured at optimal doping ($p \simeq 0.18$)[37]. The dashed lines represent the expectation of Eq.4, assuming $n_H = n_s$ and two hypothetical values for m^* .

| System | T_c (K) | λ (nm) | m^* (m_e) | n_S (10^{20}cm^{-3}) | n_H (10^{20}cm^{-3}) |
|--------|--------------|-------------------|--------------------|--------------------------------------|--------------------------------------|
| STO | 0.3 | 870 | 4.2 | 1.6 | 2.1 |
| Nb | 9.3 | 31.5[31] | 1.5-4[34] | 520 | 620[36] |
| YBCO | 89 | 103[37] | 3.6[40] | 96 | 50[41] |

TABLE I: Penetration depth, superfluid density, normal-state carrier-density in three clean superconductors. Note that the largest effective mass measured in in YBCO[40] corresponds to $p=0.15$, below optimal doping ($p=0.18$).

Fig4a shows the ratio of the extracted n_s over the normal state carrier density n_H for our six samples. Note that the total number of carriers residing in different Fermi surface pockets and detected by quantum oscillations, n_{SDH} [9] matches n_H extracted from Hall coefficient. Therefore, there is little doubt that n_H effectively yields the concentration of carriers in the normal state. As seen in this figure, the superfluid density and the normal carrier density match each other at low doping. A deviation starts at optimal doping before drastically increasing at higher doping levels. Thus, the superfluid stiffness (that is λ^{-2}) follows the doping dependence of the critical temperature, because n_s becomes lower than n_H in the overdoped regime.

C. Discussion

Disorder can pull down n_s well below n_H by two distinct mechanisms. The first is relevant to all superconductors. Metallic conductivity has a characteristic energy scale, \hbar/τ . It increases with increasing disorder, which reduces scattering time, τ . In the Drude picture, quasi-particle conductivity is concentrated at energies below this scale. When the superconducting gap, Δ , is much larger than this energy scale, the condensate density and the density of normal quasi-particles participating in transport are comparable. In the opposite limit (that is, when $\hbar/\tau \gg \Delta$), condensation affects a small fraction of normal-state charge carriers (those with sub-gap energies) and therefore one expects $n_s \ll n_H$. This mechanism is often expressed in terms of the Ferrel-Glover-Tinkham sum rule[2, 44]. Another disorder-driven mechanism is specific to nodal superconductors like cuprates and is associated with non-magnetic pair breaking. Note that in both cases, the crossover between the two regimes is tuned by the same energy scales (\hbar/τ and Δ). Since experiments indicate that n-doped SrTiO_3 is s-wave[23, 26], only the first mechanism is relevant here.

In order to document the passage to the dirty limit, we extracted the scattering time τ from low-temperature resistivity ($1/\rho_0 = ne^2/m^*$) and estimated the magnitude of the superconducting gap using the BCS relation $\Delta \sim 1.76k_B T_c$, in agreement with tunneling experiments[10]. The product of the two tells us on which side of the clean/dirty limit the system is. Note that $\ell/\xi = \pi\Delta\tau/\hbar$.

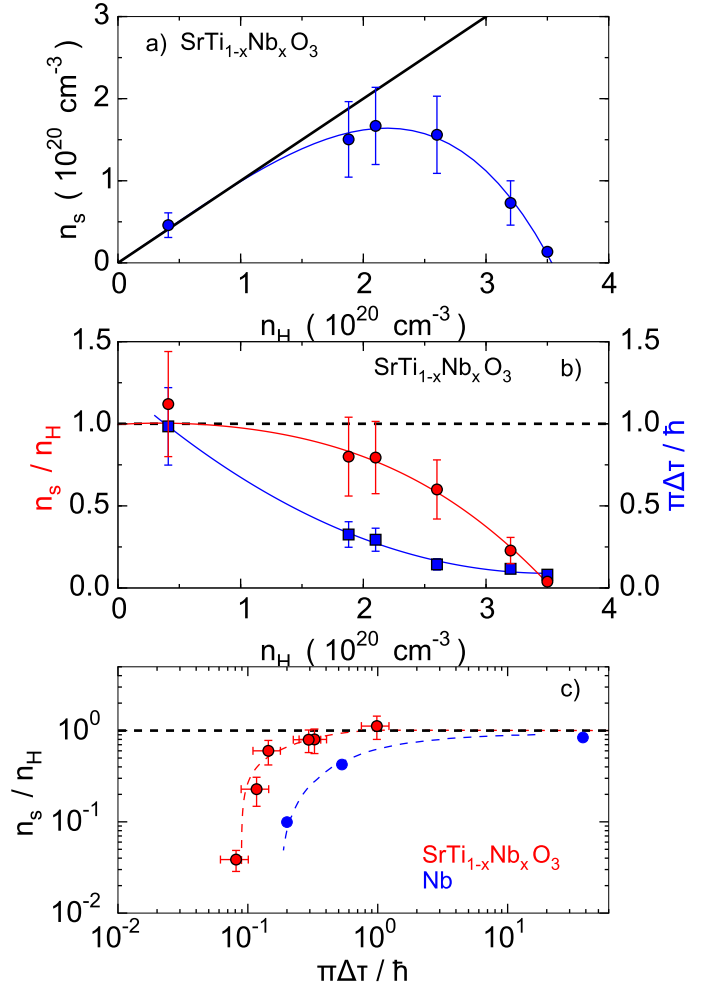


FIG. 4: **a**: Evolution of superfluid density as a function of doping. A gradual deviation from the normal-state carrier density appears at higher doping levels. **b**: The ratio of superfluid density over normal-state carrier density (red discs) compared with the product of the scattering time and the superconducting gap (blue squares) as a function of doping. Lines are guides to the eye. **c**: The evolution of superfluid density in Nb (blue squares[31, 42, 43]) and in Nb-doped SrTiO_3 (red discs) as the two system enter the dirty limit.

When $\pi\Delta\tau/\hbar$ exceeds unity, one enters the dirty limit. Fig.4b. compares the evolution of n_s/n_H and $\pi\Delta\tau/\hbar$. The two quantities deviate from unity concomitantly, but are not proportional to each other in the dirty limit as one may expect in the crudest conceivable approximation. It is also instructive to compare our data with available data on Nb from three different studies[31, 42, 43]. Putting these results together, one sees that the clean-to-dirty crossover and the loss of superfluid density are concomitant[2]. Figure 4.c shows the variation of n_s/n_H with $\pi\Delta\tau/\hbar$ in $\text{SrTi}_{1-x}\text{Nb}_x\text{O}_3$ and in Nb. The qualitative similarity and the quantitative difference indicate that a comprehensive theory of the loss of superfluid density with disorder is still missing.

Let us summarize our main conclusions. First, super-

| Sample | n_H (10^{20} cm^{-3}) | T_c (mK) | H_{c1} (Oe) | H_{c2} (Oe) | κ | λ (nm) | n_s (10^{20} cm^{-3}) | ρ_{2K} ($\mu\Omega\cdot\text{cm}$) | τ (ps) | $\frac{n_s}{n_H}$ | $\frac{\pi\Delta\tau}{\hbar}$ |
|--------|--|---------------|------------------|------------------|----------|-------------------|--|--|-------------------|-------------------|-------------------------------|
| STO | 0.41 | 183 | 1.6 | - | - | 1607 | 0.46 | 49 | 7.43 | 1.12 | 0.980 |
| | 1.9 | 300 | 5.26 | - | - | 886 | 1.52 | 53 | 1.50 | 0.80 | 0.326 |
| | 2.1 | 303 | 5.40 | 240 | 7.5 | 873 | 1.56 | 71 | 1.34 | 0.74 | 0.294 |
| | 2.6 | 382 | 6.15 | 480 | 10.6 | 873 | 1.56 | 109 | 0.52 | 0.60 | 0.144 |
| | 3.2 | 192 | 2.85 | 210 | 10.3 | 1278 | 0.73 | 56 | 0.84 | 0.23 | 0.116 |
| | 3.5 | 118 | 0.60 | 85 | 15.1 | 2966 | 0.14 | 45 | 0.95 | 0.04 | 0.081 |
| Nb | 620 | 9.3 K | 1800 | 4000 | 0.85 | 31.5 | 520 | $2 \cdot 10^{-4}$ | 5.8 | 0.84 | 38 |
| | 620 | 9.3 K | - | - | - | 44 | 264 | 1.2 | $8 \cdot 10^{-2}$ | 0.42 | 0.53 |
| | 620 | 8.3 K | - | - | - | 90 | 63 | 3.9 | $3 \cdot 10^{-2}$ | 0.10 | 0.20 |

TABLE II: All relevant values we obtained for $\text{SrTi}_{1-x}\text{Nb}_x\text{O}_3$, and the same set of characteristic values drawn from literature for Nb samples with different level of disorder. Values for the cleanest Nb are taken from [31, 32], for the second one from [42] and for the last one from [43].

conducting $\text{SrTi}_{1-x}\text{Nb}_x\text{O}_3$ has a dome-like λ^{-2} reminiscent of cuprates. Second, comparing three different systems, one sees that when a superconductor is clean, its λ is primarily set by its carrier density and not by its critical temperature. Third, the density mismatch between superconducting and normal states is concomitant with the entry to the dirty limit. Since in all superconducting domes, the T_c and the gap eventually vanish by overdoping, the mismatch should be generic to all superconducting domes. Finally, a quantitative account of the missing superfluid requires consideration of energy scales other than Δ and τ/\hbar . In the case of $\text{SrTi}_{1-x}\text{Nb}_x\text{O}_3$, the small plasma energy may prove to be a relevant quantity.

We thank A. J. Millis, J. Orenstein and L. Taillefer for helpful discussion and comments. This work is supported by Agence Nationale de la Recherche through the QUANTUM LIMIT project, by Fonds-ESPCI-Paris and by JEIP-Collège de France. We also acknowledge a recent microwave study by Thiemmann and co-workers[45], which was brought to our attention before the submission of this paper.

D. Materials and Methods

We measured the lower critical field with Hall devices realized using a high-mobility Al(Ga)As heterostructure with a two-dimensional electron gas (2DEG) 160 nm below the surface. The 2DEG has a mobility of $320,000 \text{ cm}^2/\text{Vs}$ and a carrier density of $2 \times 10^{11} \text{ cm}^{-2}$ at liquid-helium temperature. The devices were fabricated using electron beam lithography and 250V argon ions to define the mesa.

The Hall resistance of a 2DEG probe yields the local magnetic field, B :

$$R_{xy,probe} = B/ne \quad (5)$$

Here n is the carrier density of the electron gas. In our case with $1/ne \sim 0.3\Omega/\text{G}$, we could easily resolve very

small variations in magnetic field. We checked that the $1/ne$ coefficient does not change with temperature below 1 K. To measure H_{c1} , the sample is laid on the array as depicted in the inset of Fig.1a. At low field, the sample is in the Meissner state and the probes below do not feel any magnetic field, which is screened by the sample. When the first vortex penetrates the sample, the microprobe detects a rise in the measured magnetic field. The field value at which it occurs gives the penetration field H_p . The data for one sample at one temperature, presented in Fig.1a, illustrates how clearly one can detect H_p .

We monitored the Hall resistance of several probes in the proximity of the sample edges. Our data is based on a probe located below the sample and about $150 \mu\text{m}$ distant from the edge. We chose this option to avoid two phenomena, which can disrupt an accurate determination of H_{c1} . Vortices can penetrate by the corner of the sample below H_p [18]. Therefore, the sample corners are to be avoided. On the other hand, vortex pinning may generate a non-uniform distribution of magnetic field[29]. Like a previous study[30], the probe was located close to the edge in order to avoid this. The sharpness of the increase in $R_{xy,probe}$ at H_p in our data indicates that these phenomena do not contaminate our measurements.

A perfect surface may forbid the flux lines to penetrate the sample and thus artificially increase the penetration field[27]. Experimentally, this surface barrier effect will be manifested as a slow increase above H_p and then a sharp rise when the barrier is overcome[18]. Such effect is absent from our data (see Fig.1a). Most probably, this is because the surface roughness of our samples is of the same order as the penetration depth[28].

Another experimental challenge is the presence of residual and Earth magnetic field. Their magnitude are not negligible compared to the lower critical field measured here. We compensated them by applying a small magnetic field. As seen in Fig. 1, the magnitude of H_p was identical for the two field polarities. The small asymmetry for the most overdoped sample quantifies the limits

of our compensation method.

-
- [1] Y. J. Uemura *et al.* Universal correlations between T_c and $\frac{n_s}{m^*}$ (carrier density over effective mass) in high- T_c cuprate superconductors. *Phys. Rev. Lett.* **62**, 2317 (1989)
 - [2] C. C. Homes, S. V. Dordevic, T. Valla, and M. Strongin. Scaling of the superfluid density in high-temperature superconductors. *Phys. Rev. B* **72**, 134517 (2005)
 - [3] I. Božović, X. He, J. Wu and A. T. Bollinger. Dependence of the critical temperature in overdoped copper oxides on superfluid density. *Nature* **536**, 309 (2016)
 - [4] E. Bustarret. Superconductivity in doped semiconductors. *Physica C* **514**, 36 (2015)
 - [5] J. F. Schooley, W. R. Hosler, and M. L. Cohen. Superconductivity in Semiconducting SrTiO₃. *Phys. Rev. Lett.* **12**, 474 (1964)
 - [6] J. F. Schooley *et al.* Dependence of the superconducting transition temperature on carrier concentration in semiconducting SrTiO₃. *Phys. Rev. Lett.* **14**, 305 (1965)
 - [7] C. S. Koonce, M. L. Cohen, J. F. Schooley, W. R. Hosler and E. R. Pfeiffer Superconducting transition temperatures of semiconducting SrTiO₃. *Phys. Rev.* **163**, 380 (1967)
 - [8] X. Lin, Z. Zhu, B. Fauqué, and K. Behnia. fermi surface of the most dilute superconductor. *Phys. Rev. X* **3**, 021002 (2013)
 - [9] X. Lin *et al.* Critical Doping for the onset of a two-Band superconducting ground state in SrTiO_{3- δ} . *Phys. Rev. Lett.* **112**, 207002 (2014)
 - [10] G. Binnig, A. Baratoff, H. E. Hoenig and J. G. Bednorz. Two-band superconductivity in Nb-doped SrTiO₃. *Phys. Rev. Lett.* **45**, 1352 (1980)
 - [11] T. R. Lemberger, I. Hetel, A. Tsukada, M. Naito, and M. Randeria. Superconductor-to-metal quantum phase transition in overdoped La_{2-x}Sr_xCuO₄. *Phys. Rev. B* **83**, 140507(R) (2011)
 - [12] K. Behnia, C. Capan, D. Mailly, and B. Etienne. Internal avalanches in a pile of superconducting vortices. *Phys. Rev. B* **61**, R3815(R) (2000)
 - [13] R. Okazaki *et al.* Anomalous temperature dependence of lower critical field in ultraclean URu₂Si₂. *J. Phys. Soc. Jpn.* **79**, 084705 (2010)
 - [14] C. Putzke *et al.* Anomalous critical fields in quantum critical superconductors. *Nature Commun.* **5**, 5679 (2014)
 - [15] E. H. Brandt. Irreversible magnetization of pin-free type-II superconductors. *Phys. Rev. B* **60**, 11939 (1999)
 - [16] E. H. Brandt. The flux-line lattice in superconductors. *Rep. Prog. Phys.* **58**, 1465 (1995)
 - [17] E. Ambler, J. H. Colwell, W. R. Hosler, and J. F. Schooley. Magnetization and critical fields of superconducting SrTiO₃. *Phys. Rev.* **148**, 280 (1966)
 - [18] R. Liang, P. Dosanjh, D. Bonn, W. Hardy, and A. Berlinsky. Lower critical fields in an ellipsoid-shaped YBa₂Cu₃O_{6.95} single crystal. *Phys. Rev. B* **50**, 4212 (1994).
 - [19] M. Tinkham. Introduction to superconductivity (McGraw-Hill, New York, 1975), Chap. 5.
 - [20] J. L. Harden and V. D. van Arp. The lower critical field in the Ginzburg-Landau theory of superconductivity. *Cryogenics* **3**, 105 (1963)
 - [21] C.-R. Hu. Numerical constants for isolated vortices in superconductors. *Phys. Rev. B* **6**, 1756 (1972)
 - [22] R. A. Klemm and J. R. Clem. Lower critical field of an anisotropic type-II superconductor. *Phys. Rev. B* **21**, 1868 (1980)
 - [23] X. Lin *et al.* Multiple nodeless superconducting gaps in optimally doped SrTi_{1-x}Nb_xO₃. *Phys. Rev. B* **90**, 140508 (2014)
 - [24] D. van der Marel, J. L. M. van Mechelen, and I. I. Mazin. Common Fermi-liquid origin of T^2 resistivity and superconductivity in n-type SrTiO₃. *Phys. Rev. B* **84**, 205111 (2011)
 - [25] Y. J. Chang, A. Bostwick, Y. S. Kim, K. Horn and E. Rotenberg. Structure and correlation effects in semiconducting SrTiO₃. *Phys. Rev. B* **81**, 235109 (2010)
 - [26] X. Lin, C. W. Rischau, C. J. van der Beek, B. Fauqu, and K. Behnia. s-wave superconductivity in optimally doped SrTi_{1-x}Nb_xO₃ unveiled by electron irradiation. *Phys. Rev. B* **92**, 174504 (2015)
 - [27] C. P. Bean and J. D. Livingston. Surface barrier in type-II superconductors. *Phys. Rev. Lett.* **12**, 14 (1964)
 - [28] L. Burlachkov, Y. Yeshurun, M. Konczykowski, and F. Holtzberg. Explanation for the low-temperature behavior of H_{c1} in YBa₂Cu₃O₇. *Phys. Rev. B* **45**, 8193 (1992)
 - [29] C. P. Bean. Magnetization of high-field superconductors. *Rev. Mod. Phys.* **36**, 31 (1964)
 - [30] R. Okazaki *et al.* Lower critical fields of superconducting PrFeAsO_{1-y} single crystals. *Phys. Rev. B* **79**, 064520 (2009)
 - [31] C. Varmazis and M. Strongin. Inductive transition of niobium and tantalum in the 10-MHz range. I. Zero-field superconducting penetration depth. *Phys. Rev. B* **10**, 1885 (1974)
 - [32] V. R. Karasik and I. Y. Shebalin. Superconducting properties of pure niobium. *JETP* **30**, 1068 (1970)
 - [33] G. B. Scott and M. Springford. The Fermi surface in niobium. *Proc. Royal Soc. A* **320**, 115 (1970)
 - [34] D. P. Karim, J. B. Ketterson and G. W. Crabtree. A de Haas-van Alphen study of niobium: Fermi surface, cyclotron effective masses, and magnetic breakdown effects. *J. Low. Temp. Phys.* **30**, 389 (1978)
 - [35] L. F. Mattheiss. Electronic structure of niobium and tantalum. *Phys. Rev. B* **1**, 373 (1970)
 - [36] J. le G. Gilchrist and J.-C. Vallier. Hall effect in superconducting niobium and alloys. *Phys. Rev. B* **3**, 3878 (1971)
 - [37] T. Pereg-Barnea, P. J. Turner, R. Harris, G. K. Mullins, J. S. Bobowski, M. Raudsepp, Ruixing Liang, D. A. Bonn, and W. N. Hardy. Absolute values of the London penetration depth in YBa₂Cu₃O_{6+y} measured by zero field ESR spectroscopy on Gd doped single crystals. *Phys. Rev. B* **69**, 184513 (2004)
 - [38] D. N. Basov *et al.* Disorder and superconducting-state conductivity of single crystals of YBa₂Cu₃O_{6.95}. *Phys. Rev. B* **49**, 12165 (1994)
 - [39] W. J. Padilla *et al.* Constant effective mass across the phase diagram of high- T_c cuprates. *Phys. Rev. B* **72**, 060511(R) (2005)

- [40] B. J. Ramshaw *et al.* Quasiparticle mass enhancement approaching optimal doping in a high- T_c superconductor. *Science* **348**, 317 (2015)
- [41] S. Badoux *et al.* Change of carrier density at the pseudogap critical point of a cuprate superconductor. *Nature* **531**, 210214 (2016)
- [42] O. Klein, E. J. Nicol, K. Holczer, and G. Grüner. Conductivity coherence factors in the conventional superconductors Nb and Pb. *Phys. Rev. B* **50**, 6307 (1994)
- [43] A. V. Pronin *et al.* Direct observation of the superconducting energy gap developing in the conductivity spectra of niobium. *Phys. Rev. B* **57**, 14416 (1998)
- [44] M. Tinkham and R. A. Ferrell. Determination of the superconducting skin depth from the energy gap and sum rule. *Phys. Rev. Lett.* **2**, 331(1959)
- [45] M. Thiemann, M. H. Beutel, M. Dressel, D. M. Broun, E. Fillis-Tsirakis, H. Boschker, J. Mannhart and M. Scheffler, preprint